PLOS ONE

RESEARCH ARTICLE

Will higher traffic flow lead to more traffic conflicts? A crash surrogate metric based analysis

Yan Kuang[1,2], **Xiaobo Qu**[2], **Yadan Yan**[3]*

1 Griffith School of Engineering, Griffith University, Gold Coast, Queensland, Australia, **2** School of Civil and Environmental Engineering, University of Technology Sydney, Sydney, New South Wales, Australia, **3** School of Civil Engineering, Zhengzhou University, Zhengzhou, Henan, China

* wenhee@163.com

Abstract

In this paper, we aim to examine the relationship between traffic flow and potential conflict risks by using crash surrogate metrics. It has been widely recognized that one traffic flow corresponds to two distinct traffic states with different speeds and densities. In view of this, instead of simply aggregating traffic conditions with the same traffic volume, we represent potential conflict risks at a traffic flow fundamental diagram. Two crash surrogate metrics, namely, Aggregated Crash Index and Time to Collision, are used in this study to represent the potential conflict risks with respect to different traffic conditions. Furthermore, Beijing North Ring III and Next Generation SIMulation Interstate 80 datasets are utilized to carry out case studies. By using the proposed procedure, both datasets generate similar trends, which demonstrate the applicability of the proposed methodology and the transferability of our conclusions.

Citation: Kuang Y, Qu X, Yan Y (2017) Will higher traffic flow lead to more traffic conflicts? A crash surrogate metric based analysis. PLoS ONE 12(8): e0182458. https://doi.org/10.1371/journal.pone.0182458

Editor: Xiaolei Ma, Beihang University, CHINA

Received: April 10, 2017

Accepted: July 18, 2017

Published: August 7, 2017

Data Availability Statement: All relevant data are within the paper and its Supporting Information files.

Funding: This research is supported by UTS FEIT blue sky scheme.

Competing interests: The authors have declared that no competing interests exist.

Introduction

Due to the massive losses caused by road crashes, traffic safety has become a high-priority issue to traffic researchers and engineers [1–4]. As highlighted in an overview paper by Lord and Mannering [5], many generalized linear regression models were developed to establish the relationship between crash count, traffic parameters and road geometry parameters. Among such research, a considerable amount of pioneering studies have been conducted addressing the relationship between historical crash data and traffic volume, using different forms of traffic volume, such as Annual Average Daily Traffic (AADT), the hourly traffic volume and the volume/capacity (V/C) ratio [6–18]. Many different models have been developed to represent the relationship between the traffic volume and crash data, either linearly or non-linearly. Tanner [19] found that the traffic volume and crash data followed the model $Y = \alpha F^{\beta}$, where Y represented the crash count, F denoted the traffic volume, and α, β were the calibration coefficients. A non-linear concave function was found by Hauer and Persaud [20] to represent this relationship. Abbas [21] concluded that it followed a power function for most rural roads in Egypt. A typical U-shaped relationship was constructed in some other studies [22–25].

One particular traffic volume corresponds to two distinct traffic states with different densities and speeds in the fundamental diagram [26–28]. Although these two states have the same volume, it is of significance to distinguish them when analysing the relationship between traffic volume and crash. It is widely accepted that traffic volume itself is inappropriate to represent a traffic state [29–31]. Other traffic flow characteristics such as speed and/or density should be considered when establishing the relationship between traffic conditions and potential conflict risks. This relationship should be formulated based on the actual crash data. However, large amounts of quality crash data in some traffic conditions are usually absent in practice, making it difficult to represent flow—crash relationship cross all traffic conditions. Hence, in this research, we decide to use crash surrogate metrics to represent potential conflict risks, since crash surrogates have more frequent occurrence [32–37]. Many crash surrogate metrics have been proposed and applied to measure traffic conflict risks in existing studies [38–47].

We examine the relationship between traffic flow and potential conflict risk by using two prominent crash surrogate metrics, namely, Aggregated Crash Index and Time to Collision. Case studies are then carried out based on the Beijing North Ring III and Next Generation SIMulation Interstate 80 datasets. Using the proposed procedure, both datasets generate similar flow—conflict risk trends, which demonstrate the applicability of the proposed methodology and the transferability of our conclusions.

Surrogate metrics

Aggregated Crash Index (ACI)

The ACI is a tree-structured crash surrogate metric proposed by Kuang et al. [48], through imposing a hypothetical disturbance to the leading vehicle in a car-following scenario. Eight possible conflict types are defined by four levels of conditions, as shown in Table 1, where d_1 is the degree of disturbance; $D_{1-2}(0)$ is the initial distance gap; $V_1(0)$ and $V_2(0)$ are the initial speed for leading and following vehicle respectively; $\Delta V(0)$ is the initial speed difference. The ACI represents the accumulation of the crash risk of all possible crash outcomes. Mathematically, the ACI can be represented as

$$ACI = \sum_{j=1}^{8} CR_{L_j} = \sum_{j=1}^{8} P(L_j) \cdot C_{L_j} \tag{1}$$

where C_{L_j} and CR_{L_j} are the crash risk and the crash outcomes incurred at each leaf node L_j of tree structure which is shown in Table 1. The ACI thus directly represents the potential conflict risk, considering additional factors such as reaction time and braking capacity. For any car-following scenario i, the ACI over the time period T can be represented as

$$ACI_i = \frac{\sum_{t=0}^{N} ACI_i(t) \cdot \Delta t}{T} \tag{2}$$

where $ACI_i(t)$ denotes the ACI value for the ith car-following scenario at discrete time t; N and Δt are the total number and duration of the time intervals; T is the total time duration investigated, $T = N \cdot \Delta t$.

Time to Collision (TTC)

Time to Collision (TTC) is another widely used crash surrogate metric, which is defined as the time remains until a collision between two vehicles would have occurred if the collision course

Table 1. Leaf nodes of the tree structure [48].

Conflict type	Condition level 1 $\tau^1 = (T_1$ *vs.* $R)$	Condition level 2 $\tau^2 = (T_{A/B}$ *vs.* $R)$	Condition level 3 $\tau^3 = (TTC(R)$ *vs.* $(T_1 - R)/2)$	Condition level 4 $\tau^4 = (BRAD_{1/2}$ *vs.* $MADR)$	Leaf node L_j	Probability $P(L_j)$	Outcome C_{L_j}
A1	$R \geq T_1$	$R \geq T_A$	—	—	L_1	$P(L_1)$	1
B1	$R < T_1$	$R \geq T_B$	—	—	L_4	$P(L_4)$	1
A211	$R \geq T_1$	$R < T_A$	$TTC(R) \geq (T_1 - R)/2$	$BRAD_1 > MADR$	L_2	$P(L_2)$	1
A210	$R \geq T_1$	$R < T_A$	$TTC(R) \geq (T_1 - R)/2$	$BRAD_1 \leq MADR$	L_3	$P(L_3)$	0
B211	$R < T_1$	$R < T_B$	$TTC(R) \geq (T_1 - R)/2$	$BRAD_1 > MADR$	L_6	$P(L_6)$	1
B210	$R < T_1$	$R < T_B$	$TTC(R) \geq (T_1 - R)/2$	$BRAD_1 \leq MADR$	L_5	$P(L_5)$	0
B220	$R < T_1$	$R < T_B$	$TTC(R) < (T_1 - R)/2$	$BRAD_2 \leq MADR$	L_7	$P(L_7)$	0
B221	$R < T_1$	$R < T_B$	$TTC(R) < (T_1 - R)/2$	$BRAD_2 > MADR$	L_8	$P(L_8)$	1

Notations: R: reaction time of the following vehicle; T_1: stopping time of leading vehicle; T_A: value of $\frac{D_{1-2}(0)+\frac{V_1^2(0)}{2d_1}}{V_2(0)}$; T_B: value of $\frac{\sqrt{\Delta V^2(0)+2d_1 \cdot D_{1-2}(0)}-\Delta V(0)}{d_1}$; $P(L_j)$: probability of conflict L_j in car-following scenario i; *BRAD*: the minimum deceleration rate required to avoid a collision; *MADR*: the maximum available deceleration rate.

$BRAD_1$ is suitable for the situation where the leading vehicle stops earlier than or at the same as the following vehicle, while $BRAD_2$ works for the scenario where the following vehicle stops before the leading vehicle.

https://doi.org/10.1371/journal.pone.0182458.t001

and speed difference are maintained [38], mathematically,

$$TTC = \begin{cases} \dfrac{D_{1-2}}{v_2 - v_1}, & \text{if } v_2 > v_1 \\ \infty, & \text{otherwise} \end{cases} \tag{3}$$

At a particular time, D_{1-2} represents the distance gap of the leading and following vehicles; v_1 and v_2 denote the speeds of the leading and following vehicles. This metric has been widely applied in evaluating the level of safety in different traffic situations [49, 50].

Methodology

In this research, we intend to demonstrate potential conflict risks with respect to different traffic conditions in a traffic flow fundamental diagram. In this regard, we need to divide all data into many distinct traffic conditions with different flow characteristics and conflict risks. Firstly, the traffic conflict risk of each car-following scenario can be estimated by using the ACI and TTC, based on the collected traffic data (i.e., speeds, vehicle lengths and time headways). Those original traffic data of car-following scenarios are then integrated into many aggregated points with respect to different traffic conditions. The potential conflict risk of each aggregated traffic point is calculated based on the number of car-following scenarios involved in each 60-second time period. Finally, those aggregated traffic points are divided into many traffic states, sorted by density, with uniform span.

Traffic conflict data

As suggested by previous researchers [51, 52], the distance headway for a car-following scenario D_{1-2} can be estimated by $(V_2 \times h_2 - l_1)$. l_1 denotes the length of the leading vehicle in the car-following scenario, while V_2 and h_2 represent the speed and time headway of the following vehicles at a particular time, respectively.

As our road section is rather short, we assume the traffic flow in this road section is homogeneous with a similar traffic flow characteristics. In other words, we can simply measure the

potential conflict risk at a particular spot, and use aggregated risk over time to represent the risk values for this short road section in the given time period. In this research, ACI can represent the risk directly, while the risks represented by TTC are determined by comparing their values and thresholds. Mathematically,

$$IR_{ij} = \begin{cases} S_j^* - S_{ij}, & \text{if } S_j^* > S_{ij} \\ 0, & \text{otherwise} \end{cases} \tag{4}$$

where IR_{ij} represents the Individual Risk (IR) of discrete car-following scenario i measured by surrogate j; S_{ij} denotes the surrogate value for discrete scenario i measured by surrogate j; S_j^* is the threshold of surrogate metric j. As suggested by Kuang et al. [46, 48], the thresholds of TTC and ACI are adopted as 4s and 0, respectively. Accordingly, the traffic conflict risk of each car-following scenario can be measured by using surrogate metrics ACI and TTC.

Aggregated traffic points

Each aggregated traffic point is calculated based on the number of vehicles passing through the road section in each 60-second time period. The aggregated traffic density, speed and conflict refer to the average values of the source data involved in each time period. Similarly, the integrated conflict risk of each aggregated traffic point can be represented by the ACI and TTC, respectively.

Traffic states

In order to examine the relationship between traffic conflict risk and traffic state, we adopt the following procedure to divide the field data into many traffic states, sorted by density, with uniform span.

Step 1. Rank all observations according to their densities, from smallest to largest,

$$(k_{(1)}, v_{(1)}, f_{(1)}, IR_{(1)}),\ \cdots, (k_{(i)}, v_{(i)}, f_{(i)}, IR_{(i)}), \cdots,\ (k_{(m)}, v_{(m)}, f_{(m)}, IR_{(m)}) \tag{5}$$

where $k_{(1)} \leq \cdots \leq k_{(i)} \leq \cdots \leq k_{(m)}$, and $v_{(i)}$, $f_{(i)}$ and $IR_{(i)}$ are, respectively, the corresponding speed, flow rate and IR value under traffic density $k_{(i)}$.

Step 2. Determine the total number of intervals for those observations with constant span δ which is set as 1.5 veh/km, mathematically

$$\tilde{n} = \text{round}\left(\frac{k_{\max} - k_{\min}}{\delta}\right) \tag{6}$$

where $\tilde{n}$ is the total number of intervals, and $k_{\max}$ and $k_{\min}$ represent the maximum and minimum density of the data, respectively.

Step 3. Find the range of each interval as follows:

$$(k_{\min} + \delta \cdot (n-1),\ k_{\min} + \delta \cdot n],\ \ n \in (1:1:\tilde{n}) \tag{7}$$

Then count and record the number of data points for the corresponding interval as

$$N_n,\ \ n \in (1:1:\tilde{n}) \tag{8}$$

Step 4. Calculate the Cumulative Risk (CR) value for each interval, which can be written as

$$CR_n = \sum_{i=M_{n-1}}^{M_{n-1}+N_n} IR_i,\ M_{n-1} = \sum_{n=1}^{n-1} N_n,\ n \in (1:1:\tilde{n}) \tag{9}$$

where CR_n denotes the CR value for the nth interval, while M_{n-1} and IR_i respectively denote the lower bound of the nth interval and the ith IR value in step 1.

Step 5. Compute the Average Risk (AR) value for each interval as follows:

$$AR_n = {}^{CR_n}/_{N_n},\ n \in (1:1:\tilde{n}) \tag{10}$$

where AR_n and N_n are the AR and the total number of i for the nth interval.

Data collection

Two distinct datasets are used to demonstrate our potential risk flow relationship. Data I was collected on the North Ring III expressway in Beijing, China, and data II was gathered from the interstate 80 freeway in the San Francisco Bay area in Emeryville, CA, USA.

Data I—Beijing North Ring III expressway

Data I (S1 File) was collected on June 21st (Tuesday) in 2011, during eight different time periods including two morning peak hours, three afternoon peak hours, and three off-peak hours. There are three lanes with speed limit of 80 km/hour at the spot. During the data collection, there were no traffic crash occurred. By taking advantage of the video recording systems, the traffic volumes, density spot speeds, time headways and vehicle lengths were recorded. Total 52,994 original car-following scenarios are used. Those original data are moreover integrated into 2,280 aggregated traffic data samples.

Data II—NGSIM interstate 80 freeway

The data of Interstate 80 (I-80) Freeways was collected by the Next Generation SIMulation (NGSIM) program on eastbound I-80 in the San Francisco Bay area in Emeryville, CA, USA on April 13, 2005. As stated by [53], the study area was approximately 500 meters (1,640 feet) in length and consisted of six freeway lanes, including a high-occupancy vehicle (HOV) lane, with speed limit of 110 km/h. A total of 45 minutes of trajectory data are available in the full dataset, segmented into three 15-minute periods: 4:00 p.m. to 4:15 p.m.; 5:00 p.m. to 5:15 p.m.; and 5:15 p.m. to 5:30 p.m., by using seven cameras. We further extracted total 139,230 car-following scenarios from the trajectory data. 4,644 aggregated traffic data samples are generated on the basis of those source car-following scenarios data.

It is found that the speed and density of both data follow the Underwood model [54]. The free flow speed and capacity density are estimated as 107.6 km/h and 51.9 veh/km, 181.8 km/h and 37.7 veh/km for data I and II, respectively. Fig 1 shows the characteristics of the aggregated data for both datasets in a speed-flow fundamental diagram. As can be seen in Fig 1, two data have distinct characteristics and distributions in speed and density. Data I is evenly distributed from density 20 veh/km to 100 veh/km, while data II is more concentrated in the range of density 20 veh/km to 40 veh/km. Those distinct flow characteristics are caused by the different speed limit, data collection time period and traffic conditions.

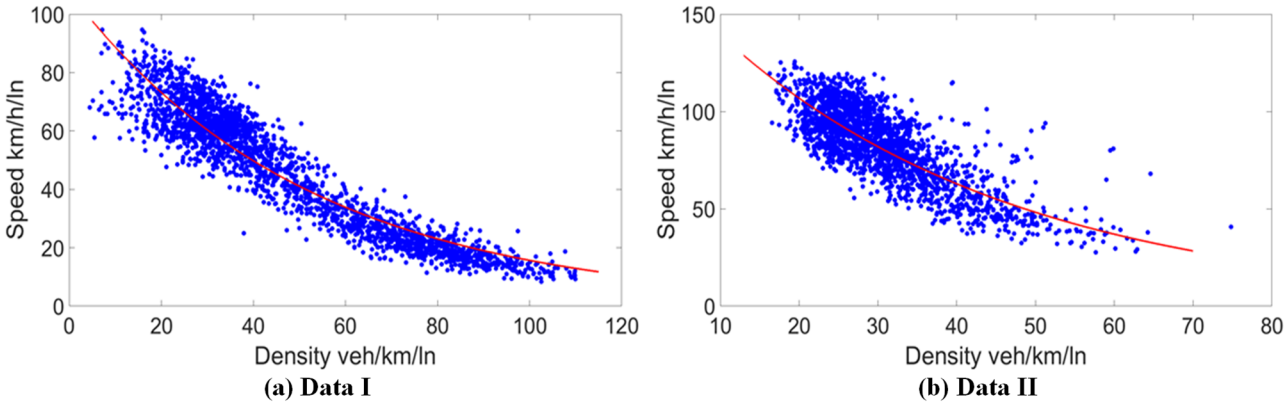

Fig 1. Aggregated traffic data in speed-density diagram for data I and II.

https://doi.org/10.1371/journal.pone.0182458.g001

Potential risk—Flow relationship

By using the methodology mentioned, the traffic states can be generated by using the aggregated traffic points. Accordingly, the density, flow, speed and conflict risk of each traffic state is estimated based on those characters of aggregated traffic points. Regarding each interval as a unique traffic state, total 70 and 39 traffic states are generated for data I and II, respectively. All traffic states are distinguished by their traffic flow characteristics and AR represented by the ACI and TTC. In order to better demonstrate the relationship between conflicts and traffic states, the curve of speed and flow are generated based on the Underwood model obtained previously. We further map the risk of each state to the corresponding position on the speed-density curve, using the AR value to determine the size and color of each point. Accordingly, the traffic conflict risk can be visually mapped onto the corresponding position in the speed-density fundamental diagram.

Fig 2 shows the speed-density diagram mapped with traffic conflict risk represented by the ACI and TTC, respectively. The bigger size and darker color of a point indicate the higher potential conflict risk of a traffic state. Obviously, the traffic conflict risk increases with an increase in density and a decrease in speed. When the density increases, the distance headways between cars are reduced, with a potential to increase the risk even though the speed decreases. As can be seen in Figs 2 and 3, the ACI has more obvious trend on the change of risks than the TTC for both data.

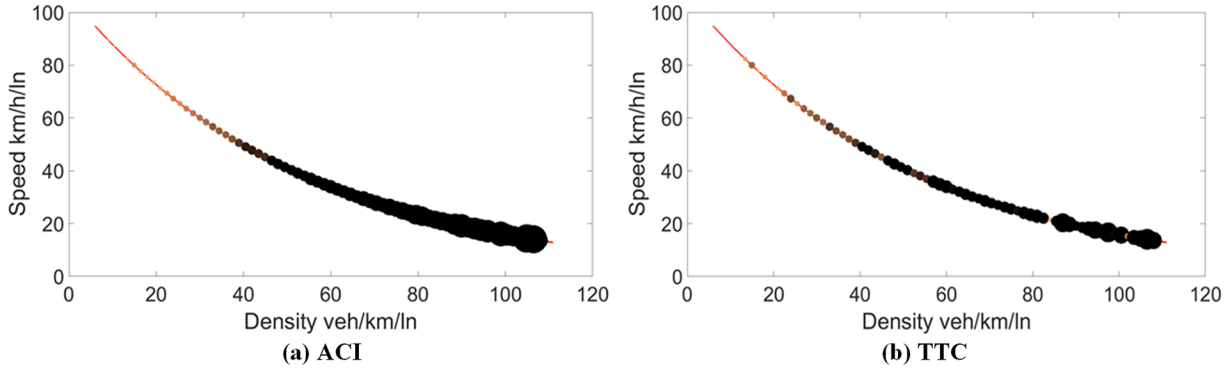

Fig 2. Traffic conflict risk on speed-density curve for data I.

https://doi.org/10.1371/journal.pone.0182458.g002

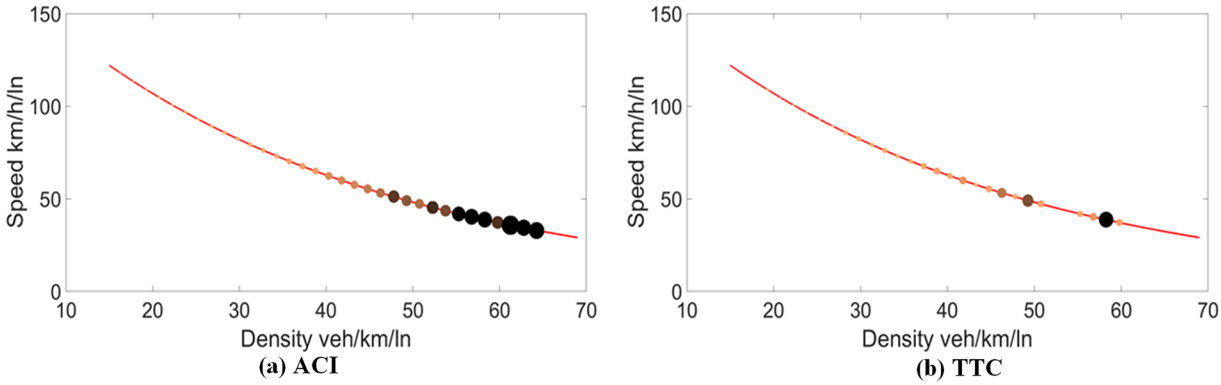

Fig 3. Traffic conflict risk on speed-density curve for data II.

https://doi.org/10.1371/journal.pone.0182458.g003

We further use the same method to map the traffic conflict risk of different states on the speed-density curve, using the risk represented by the ACI and TTC to determine the size and colour of each point. Figs 4 and 5 show the fundamental diagrams mapped with traffic conflict risk represented by the ACI and TTC, for data I and II, respectively.

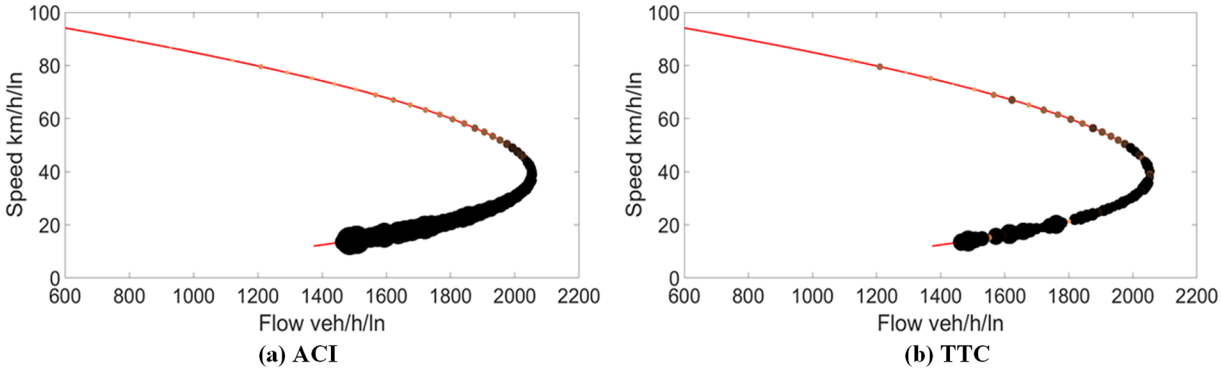

Fig 4. Traffic conflict risk on the speed-flow curve for data I.

https://doi.org/10.1371/journal.pone.0182458.g004

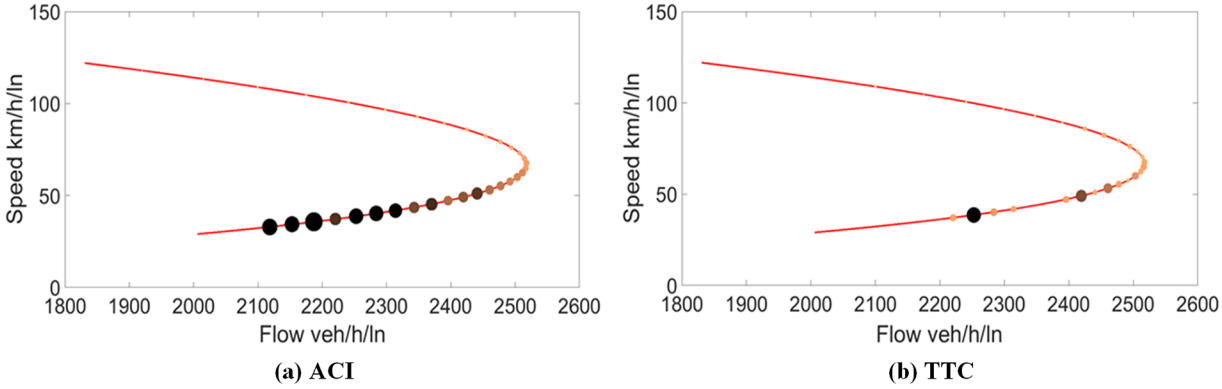

Fig 5. Traffic conflict risk on the speed-flow curve for data II.

https://doi.org/10.1371/journal.pone.0182458.g005

As depicted in Figs 4 and 5, the points are found with size increased and colour thickened as we move from top to bottom. Obviously, the potential conflict risks measured by the ACI and TTC increase when the speed decreases. As can be seen in Fig 4, the flow value located between 1,500 veh/h and capacity is found corresponding to two traffic states, with different speeds. Apparently, the traffic conflict risk is found to be distinct for those two states, the traffic conflict risk of the capacity state clearly being less than that of the over-capacity state. As can be seen in Fig 5, the conflict risk is increasing when the speed decreases along the curve from the top to the bottom in both graphs. There are two distinct traffic states found between flow rate 2,200 veh/h and capacity. The trend is also found for data II in Fig 5 by using the ACI and TTC. Thus, we can conclude that the traffic conflict risk increases along the curve, from level of service A to F. Besides, it is found that the ACI can represent the change of risks better than TTC for both data. This is consistent with that ACI has better performance than surrogate TTC by Kuang et al. [48]. The possible reasons are as follows: (1) The ACI can evaluate more car-following scenarios than TTC. According to the notions of TTC, all scenarios in which the speed of the following vehicle is not greater than that of the leading vehicle are regarded as safe. That is to say, the condition used to determine the risk is the speed differential. Thus, it is impossible to identify the risks in other scenarios by using the TTC. The ACI is based on a hypothetical disturbance; it can be used in any car-following scenario, even the leading vehicle's speed is greater than that of the following vehicle. Therefore, the ACI can have more accurate results than TTC. (2) The ACI takes more important variables into account. Since the drivers and vehicles are most critical parts in crash mechanism, the consideration of the driver's reaction time and the MADR can contribute to a better representation of the risk.

Discussion and conclusions

Since one traffic volume corresponds to two different traffic states with different speeds and densities, traffic flow itself is not able to properly represent a traffic condition. In this regard, we visualize a potential traffic risk—flow relationship in a traffic flow fundamental diagram. To this end, we use two classical surrogate metrics, namely, ACI and TTC, to represent the potential conflict risk in this study. Two distinct datasets, one collected in China and the other gathered in the U.S., are used to testify our methodology. Based on the case studies, the potential conflict risk is found to have a strong correlation with the level of service, as the latter increases from level A to F. The curves for both case studies have a similar pattern, which demonstrate the transferability of the proposed methodology.

This research has two limitations. Firstly, the sample size and data quality might not be large enough to conclude the above findings. In the future work, more data will be collected to validate the relationship that is presented in the potential risk flow relationship. Moreover, microsimulation could be used to generate simulated data for further analysis. Secondly, the study is based on the assumption that the potential conflict risk has a strong correlation with crash frequency. As a follow up study, this relationship will be validated properly using actual crash data.

Supporting information

S1 File. Data I collected from Beijing expressway.
(XLSX)

Acknowledgments

This research is supported by UTS FEIT blue sky scheme and National Natural Science Foundation of China (grant no. 51678535).

Author Contributions

Conceptualization: Yan Kuang, Xiaobo Qu.

Data curation: Yan Kuang.

Funding acquisition: Xiaobo Qu, Yadan Yan.

Methodology: Xiaobo Qu, Yadan Yan.

Supervision: Xiaobo Qu.

Validation: Xiaobo Qu.

Writing – original draft: Xiaobo Qu.

Writing – review & editing: Yadan Yan.

References

1. Ma X., Ding C., Luan S., Wang Y., Wang Y. 2017. Prioritizing influential factors for freeway incident clearance time prediction using gradient boosting decision trees method. IEEE Transactions on Intelligent Transportation Systems 99, 1–8.
2. Xu C, Liu P., Wang W., Li Z.. 2012. Evaluation of the impacts of traffic states on crash risks on freeways. Accident Analysis and Prevention 47, 162–171. https://doi.org/10.1016/j.aap.2012.01.020 PMID: 22405245
3. Mannering F.L., Bhat C.R.. 2014. Analytic methods in accident research: Methodological frontier and future directions. Analytic Methods in Accident Research 1, 1–22.
4. Ding C., Ma X., Wang Y., Wang Y.. 2015. Exploring the influential factors in incident clearance time: Disentangling causation from self-selection bias. Accident Analysis and Prevention 85, 58–65. https://doi.org/10.1016/j.aap.2015.08.024 PMID: 26373988
5. Lord D., Mannering F.. 2010. The statistical analysis of crash-frequency data: A review and assessment of methodological alternatives. Transportation Research Part A: Policy and Practice 44, 291–305.
6. Jovanis P.P., Chang H.L.. 1986. Modeling the relationship of accidents to miles travelled. Transportation Research Record 1068, 42–51.
7. Jovanis P.P., Chang H.L.. 1989. Disaggregate model of highway accident occurrence using survival theory. Accident Analysis and Prevention 21, 445–458. PMID: 2619854
8. Jovanis P.P., Chang H.L.. 1990. Formulating accident occurrence as a survival process. Accident Analysis and Prevention 22, 407–419. PMID: 2222705
9. Miaou S.P.. 1994. The relationship between truck accidents and geometric design of road sections: Poisson versus negative binomial regressions. Accident Analysis and Prevention 26, 471–482. PMID: 7916855
10. Lee C., Abdel-Aty M.. 2005. Comprehensive analysis of vehicle-pedestrian crashes at inersections in Florida. Accident Analysis and Prevention 37, 775–786. https://doi.org/10.1016/j.aap.2005.03.019 PMID: 15869737
11. Lee C., Abdel-Aty M.. 2008. Presence of passengers: Does it increase or reduce driver's crash potential. Accident Analysis and Prevention 40, 1703–1712. https://doi.org/10.1016/j.aap.2008.06.006 PMID: 18760099
12. Wong S.C., Sze N.N., Li Y.C.. 2007. Contributory factors to traffic crashes at signalized intersections in Hong Kong. Accident Analysis and Prevention 39, 1107–1113. https://doi.org/10.1016/j.aap.2007.02.009 PMID: 17920832
13. Wang C., Quddus M.A., Ison S.G.. 2009. Impact of traffic congestion on road accidents: a spatial analysis of the M25 motorway in England. Accident Analysis & Prevention 41, 798–808.
14. El-Basyouny K., Sayed T.. 2010. Application of generalized link functions in developing accident prediction models. Safety Science 48, 410–416.
15. Haque M., Chin H., Huang H.. 2010. Applying Bayesian hierarchical models to examine motorcycle crashes at signalized intersections. Accident Analysis and Prevention 42, 203–212. https://doi.org/10.1016/j.aap.2009.07.022 PMID: 19887161
16. Pei X., Wong S.C., Sze N.N.. 2011. A joint-probability approach to crash prediction models. Accident Analysis and Prevention 43, 1160–1166. https://doi.org/10.1016/j.aap.2010.12.026 PMID: 21376914

17. Lee J., Abdel-Aty M., Jiang X.. 2015a. Multivariate crash modelling for motor vehicle and non-motorized modes at the macroscopic level. Accident Analysis and Prevention 78, 146–154.
18. Lee J., Abdel-Aty M., Park J., Wang J.H.. 2015b. Development of crash modification factors for changing lane width on roadway segments suing generalized nonlinear models. Accident Analysis and Prevention 78, 146–154.
19. Tanner J.C.. 1953. Accidents at rural three-way junctions. Journal of the Institution of Highway Engineers 2, 56–67.
20. Hauer E., Persaud B.N.. 1988. How to estimate the safety of rail-highway grade crossing and the safety effects of warning devices. Transportation Research Record 1114, 131–140.
21. Abbas K.A.. 2004. Traffic safety assessment and development of predictive models for accident on rural roads in Egypt. Accident Analysis and Prevention 36, 149–163. PMID: 14642870
22. Zhou M., Sisiopiku V.P.. 1995. Relationship between volume-to-capacity ratios and accident rates. Transportation Research Record 1581, 47–52.
23. Cedar A., Livneh M.. 1982. Relationship between road accidents and hourly traffic flows—I and II. Accident Analysis and Prevention 14, 19–44.
24. Martin J.L.. 2002. Relationship between crash rate and hourly traffic flow on Interurban motorways. Accident Analysis and Prevention 34, 619–629. PMID: 12214956
25. Lord D., Manar A., Vizioli A.. 2005. Modeling crash-flow-density and crash-flow-V/C ratio relationships for rural and urban freeway segments. Accident Analysis and Prevention 37, 185–199. https://doi.org/10.1016/j.aap.2004.07.003 PMID: 15607290
26. Greenshields B.. 1937. A study in highway capacity. Highway Research Board Preceedings 14, 458.
27. Wang H., Li J., Chen Q.Y., and Ni D.. 2011. Logistic modelling of the equilibrium speed—density relationship. Transportation Research Part A: Policy and Practice 45, 554–566.
28. Qu X., Wang S., Zhang J.. 2015a. On the fundamental diagram for freeway traffic: A novel calibration approach for single-regime models. Transportation Research Part B: Methodological 73, 91–102.
29. Ma X., Tao Z., Wang Y., Yu H., Wang Y.. 2015. Long short-term memory neural network for traffic speed prediction using remote microwave sensor data. Transportation Research Part C: Emerging Technologies 54, 187–197.
30. Ma X., Dai Z., He Z., Ma J., Wang Y., Wang Y.. 2017. Learning traffic as images: A deep convolutional neural network for large-scale transportation network speed prediction. Sensors 17 (4), 818.
31. Qu X., Jin S., Weng J.. 2015b. Analysis of the relationship between aggregated traffic volume and traffic conflicts on expressways. Transportmetrica A: Transport Science 11, 648–658.
32. Kuang, Y., Qu, X., 2015. Safety fundamental diagram on freeways. CICTP 2015—Efficient, Safe, and Green Multimodal Transportation, Proceeding of the 15th COTA International Conference of Transportation Professionals, 3143–3154.
33. Chin H.C., Quek S.T.. 1997. Measurement of traffic conflicts. Safety Science 26,169–185.
34. Tarko A.P.. 2012. Use of crash surrogates and exceedance statistics to estimate road safety. Accident Analysis and Prevention 45, 230–240. https://doi.org/10.1016/j.aap.2011.07.008 PMID: 22269505
35. Wu K.F., Jovanis P.P.. 2012. Crashes and crash-surrogate events: Exploratory modeling with naturalistic driving data. Accident Analysis and Prevention 45, 507–516. https://doi.org/10.1016/j.aap.2011.09.002 PMID: 22269536
36. El-Basyouny K., Sayed T.. 2013. Safety performance functions using traffic conflicts. Safety Science 55, 160–164.
37. Alhajyassen W.K.M., Iryo-Asano M.. 2017. Studying critical pedestrian behavioral changes for the safety assessment at signalized crosswalks. Safety Science 91, 351–360.
38. Hayward, J.C., 1972. Near miss determination through use of a scale of danger (traffic records 384). Highway Research Board. Washington, DC.
39. Cooper F., Ferguson N.. 1976. Traffic studies at t-junctions—a conflict simulation model. Traffic Engineering and Control 17, 306–309.
40. Sayed T., Brown G. R., Navin F.. 1994. Simulation of traffic conflicts at unsignalised intersections with TSC-Sim. Accident Analysis and Prevention 26, 593–607. PMID: 7999204
41. Minderhoud M., Bovy P.. 2001. Extended time-to-collision measures for road traffic safety assessment. Accident Analysis and Prevention 33, 89–97. PMID: 11189125
42. Cunto F., Saccomanno F.F.. 2008. Calibration and validation of simulated vehicle safety performance at signalized intersections. Accident Analysis and Prevention 40, 1171–1179. https://doi.org/10.1016/j.aap.2008.01.003 PMID: 18460386

43. Wang C., Quddus M.A., Ison S.G.. 2013. The effect of traffic and road characteristics on road safety: A review and future research direction. Safety Science 57, 264–275.

44. Kuang Y., Qu X., Wang S.. 2014. Propagation and dissipation of crash risk on saturated freeways. Transportmetrica B: Transport Dynamics 2(3), 203–214.

45. Zheng L., Ismail K., Meng X.. 2014. Shifted Gamma-Generalized Pareto Distribution model to map the safety continuum and estimate crashes. Safety Science 64, 155–162.

46. Kuang Y., Qu X., Weng J., Etemad-Shahidi A.. 2015a. How does the driver's perception reaction time affect the performances of crash surrogate measures? PLoS ONE 10(9): e0138617. https://doi.org/10.1371/journal.pone.0138617 PMID: 26398416

47. Wang C., Stamatiadis N.. 2016. Sensitivity analysis on new simulation-based conflict metrics. Safety Science 82, 399–409.

48. Kuang Y., Qu X., Wang S.. 2015b. A tree-structured crash surrogate measure for freeways. Accident Analysis and Prevention 77, 137–148.

49. Vogel K.. 2003. A comparison of headway and time to collision as safety indicators. Accident Analysis and Prevention 35, 427–433. PMID: 12643960

50. Qu X., Yang Y., Liu Z., Jin S., Weng J.. 2014a. Potential crash risks of expressways on-ramps and off-ramps: a case study in Beijing, China. Safety Science 70, 58–62.

51. Qu X., Kuang Y., Oh E., Jin S.. 2014b. Safety evaluation for expressways: a comparative study for macroscopic and microscopic indicators. Traffic Injury Prevention 15(1), 89–93.

52. Meng Q., Qu X.. 2012. Estimation of rear-end vehicle crash frequencies in urban road tunnels. Accident Analysis and Prevention 48, 254–263. https://doi.org/10.1016/j.aap.2012.01.025 PMID: 22664688

53. FHWA, 2006. Interstate 80 Freeway Dataset. Federal Highway Administration Research and Technology Fact Sheet. Publication number: FHWA-HRT-06-137. https://www.fhwa.dot.gov/publications/research/operations/06137/

54. Underwood, R.T., 1961. Speed, volume, and density relationship: quality and theory of traffic flow. Yale Bureau of Highway Traffic, 141–188.